HIGH-SPEED IMAGING AND PIV MEASUREMENTS IN TURBULENT CAVITATING FLOWS AROUND 2D HYDROFOILS

Aleksandra Yu. Kravtsova
Institute of Thermophysics, the Russian Academy of Sciences, Siberian Branch
1, Lavrentyev Avenue, 630090, Novosibirsk, Russia

Dmitriy M. Markovich
Institute of Thermophysics, the Russian Academy of Sciences, Siberian Branch
1, Lavrentyev Avenue, 630090, Novosibirsk, Russia
Novosibirsk State University
2, Pirogova Street, 630090, Novosibirsk, Russia
Email: dmark@itp.nsc.ru

Konstantin S. Pervunin
Institute of Thermophysics, the Russian Academy of Sciences, Siberian Branch
1, Lavrentyev Avenue, 630090, Novosibirsk, Russia
Novosibirsk State University
2, Pirogova Street, 630090, Novosibirsk, Russia

Mikhail V. Timoshevskiy
Institute of Thermophysics, the Russian Academy of Sciences, Siberian Branch
1, Lavrentyev Avenue, 630090, Novosibirsk, Russia

ABSTRACT

The paper reports on high-speed imaging and PIV study of cavitating flows around a flat plate with semi-circular leading edge and a NACA0015 hydrofoil. Both foils were investigated at a series of attack angles ranging from 0 to 9° with varying cavitation number. Several known types of cavitation common to both foils, but also some different patterns, were registered. At small angles of incidence (less than 3°), cavitation on the plate begins in form of a streak array (bubble-band) whereas on the hydrofoil as travelling bubbles. For the regimes with developed cavitation on the NACA0015 hydrofoil, the scattered and discontinuous bubble streaks branch and grow but subsequently merge into bubble clouds forming a remarkably regular lattice pattern. Once the incidence angle increased to 9°, the cavitation on the hydrofoil changed to a streaky pattern like that on the plate at zero attack angle, whereas the regime on the plate showed no significant changes. The time-averaged velocity and turbulence moments show that the incipience of cavitation is governed by the development of the carrier-fluid flow around the foil leading edges, but the subsequent flow pattern depends strongly on the cavitation regime displaying markedly different distributions compared to the noncavitating case. The influence of the test object scale and the foil surface roughness on the cavitation pattern as well as on the mean velocity and turbulence intensity was analyzed. Thus, surface roughness leads to faster turbulization of the boundary layer and, consequently, to growth of the transversal dimension of the turbulent wake. Turbulent wake past the foil was shown to be wider for the larger hydrofoil due to the flow acceleration as a result of greater flow blockage.

INTRODUCTION

Flow in complex configurations of real power systems and their prime components – hydroturbines, supply ducts and draft tubes, are usually highly turbulent, unsteady and featured by large-scale vortical structures (LVS) and passive secondary motions of different origin and types. Often and especially at variable off-design loads, one unavoidably encounters cavitation and the consequent undesirable two-phase phenomena. The dispersed phase (bubbles, clouds) is governed by turbulence and the LSV dynamics (turbulent dispersion), while the bubble motion and the vapour-gas phase in general significantly changes properties of turbulent fluctuations in the carrier phase (turbulence modulation) due to a number of physical mechanisms. Nonlinear interactions of LSV with gas-vapor dispersed phase lead often to strong flow pulsations, which may come into resonance with the structures natural frequency and cause excessive vibrations and, as a consequence, failure of hydraulic equipment or, at worst, even emergencies.

The quest for improving the hydromachinery efficiency, durability and safety has necessitated ever-new studies of cavitation aimed at reducing its negative effects. More recently, these studies take the advantage of modern measuring techniques and computer simulations and are directed more towards gaining a deeper insight into physical mechanisms and processes, various regimes of cavitation and its interaction with flow of the carrier fluid. These methods make it possible to investigate simultaneously the spatial distribution and the time-dynamics of cavitation-generated gas-vapour dispersed phase, the vortical and turbulence structures of the carrier fluid and their interactions. This, in turn, should lead to better understanding

and the ability to forecast cavitation and the consequent erosion, as well as to provide guidance for their control. It is noted, however, that the methods for reducing the negative effects of cavitation have to satisfy the requirement for power loss minimization.

Despite extensive research, detailed quantitative information for cavitating flows required for design and optimization, as well as for verification of the existing and development of advanced mathematical models, is still lacking and, to a large extent, limited to simplified conditions and usually 2D geometries. Experiments on full-scale objects are very difficult or can even be impossible, but the laboratory investigations are also costly and require expensive laboratory setups. Thus, most publications in the literature report on research in simple geometries (Venturi nozzles, scaled-down shaped bodies, e.g. NACA series hydrofoils, etc.) though at varying conditions and with focus on diverse issues of the cavitation incipience and development of different regimes. The acquisition of systematic experimental data for various cavitation regimes is still an issue.

Depending on flow conditions (foil shape and surface texture, velocity and pressure fields, overall flow configuration and others), one can distinguish a variety of cavitation patterns (bubbles, vortex or cloud cavitation, supercavitation, etc.), but practically all spatial cavitation patterns can be grouped into two generic types – partial cavities and supercavities. Partial cavities occur when a cavity closes on the cavitating surface, while a supercavity closes downstream in the wake of the cavitating object. The partial cavities can further be classified into closed and open cavities, depending on the flow in the cavity closure region (Laberteaux and Ceccio, 2001). A typical example of closed cavities is the sheet cavitation whereas that of the open cavities is the cloud cavitation. A cloud cavitation arises when a large portion of vapour-filled cavity underlined with re-entrant fluid breaks off, forming a cavitation cloud.

Experimental studies report on visual observations and regime maps with qualitative descriptions (e.g. Franc and Michel, 1985), point pressure measurements (Cervone et al., 2006) and, sometimes, velocity distributions (Kubota et al., 1989). Measurements of the local volume fraction of vapor phase within a cavity and in the wake past a foil were also reported (e.g. Coutier-Delgosha et al., 2006). The impact of thermal effects on the onset of various forms of cavitation and instabilities was studied by Cervone et al. (2006), etc. Much of the works published in the literature deal with the experimental investigation of cloud cavitation (e.g. Kawanami et al., 1997 and Callenaere et al., 2001). As widely acknowledged, when a sheet cavity reaches a certain dimension, periodic oscillations of cavity appear. This process is accompanied by a cavity (in the form of clouds) shedding downstream. Kubota et al. (1989) showed that a cloud cavity consists of a large-scale vortex and a cluster of small vapor bubbles situated in the core of the vortex. In various experiments (e.g. George et al., 2000), it was revealed that cloud cavity pulsations occur at similar Strouhal numbers. Callenaere et al. (2001) proposed correlations between separation of a cloud cavity and the re-entrant jet generated in the cavity closure region due to the adverse pressure gradient.

The present paper aims at investigating the mutual impact of the flow hydrodynamics and a partial cavity initiation and detachment, as well as cloud cavity shedding on 2D hydrofoils. It also reports on the results of high-speed imaging of the cavitating foils and the PIV-measurements of spatial distributions of mean and turbulent characteristics about the foils at various flow conditions. Besides, the scale effect and test object roughness impact on the cavitation inception, cavity development and turbulence intensity distribution are of a special interest in the present work.

EXPERIMENTAL CONDITIONS AND MEASUREMENT TECHNIQUE

Experiments were carried out in the Cavitation tunnel of the Institute of Thermophysics SB RAS. Detailed description of the setup can be found in Kravtsova et al. (2012).

We investigated the spatial structure and dynamics of partial cavities and measured the velocity and turbulence intensity in flows around a 2D plate with semi-cylindrical nose and sharp-cut end (100 mm chord and 15 mm thickness), and a NACA0015 series hydrofoil (100 mm chord) at four attack angles $\alpha = 0, 3, 6$ and $9°$. The test objects were made of brass with roughness level of about 2.8 μm. In order to investigate the impact of roughness on the onset of cavitation and partial cavities development we utilized one more NACA0015 hydrofoil with roughness level of 4.5 μm as a test object. The scale effect on the cavities and turbulence intensity was studied on three NACA0015 foils with chord lengths of 50, 100 and 200 mm.

The working liquid was distilled water. The amount of dissolved air in liquid was estimated by Henry's law under the normal conditions to be approximately 0.023 g of air in 1 kg of water. The liquid temperature was kept at 30°C with uncertainty of ±0.1°C and the overpressure in the setup was fixed to 0.5 bars.

The flow regime is defined by the cavitation number, $\sigma = (P_{in} - P_V)/(\rho U_0^2/2)$, where P_{in} is the static pressure at the test section inlet, P_V is the water vapour pressure, U_0 is the bulk flow velocity. In order to observe various cavity patterns, the cavitation number was adjusted by varying the dynamic pressure, $\rho U_0^2/2$, in the range from 0.5 to 5.5. Under the present conditions, $P_V = 0.044$ bar. The initial turbulence intensity was lower than 1%. The Reynolds number, Re, based on U_0 and the chord length, C, was in the range between $0.8×10^6$ and $1.7×10^6$. The Strouhal number, St, for the nondimensional cloud shedding frequency is defined in terms of the cloud streamwise dimension D_{cl} and the cloud convection velocity U_{cl}. The uncertainties in defining of cavitation number and estimating the Reynolds and Strouhal numbers were 6%, 3% and 4%, respectively.

The dynamics and spatial structure of gas-vapor cavities was analysed by high-speed visualization using Photron FASTCAM SA5 camera at a frame rate of 20-100 kHz taken from above and from the side. The velocity fields were measured by a "PIV-IT" PIV-system consisting of a double-pulsed Nd:YAG Quantel EVG00200 laser (wavelength 532 nm, repetition rate 15 Hz, pulse duration 10 ns, pulse energy 200 mJ), a CCD-camera (10 bits per pixel, matrix resolution 2048×2048 pixels) equipped with Nikon AF Nikkor 50 mm f/1.4D lens and an optical low-pass filter (bandpass edge at 570 nm), as well as a synchronizing processor. The PIV-system was operated via a computer using "ActualFlow" software (Akhmetbekov et al., 2006). The thickness of the laser light sheet formed by a cylindrical lens to illuminate tracer particles was about 0.8 mm in the measurement plane that coincided with the central longitudinal plane of the test section parallel to its larger sidewalls. The distance between the camera and the

laser sheet was 527 mm. The size of the measurement area was approximately 124×124 mm. Since in a cavitating flow the micro-size vapour bubbles can act as tracers, their contaminating effect on the PIV measurements was reduced by adding fluorescent tracers (average size 10 µm, wavelength range 550-700 nm) into the working liquid.

RESULTS

The results of the visualization and field measurements (velocity and turbulence statistics) are given only for $\alpha = 3°$ because of the limitations of the Conference paper format. This value of the attack angle was selected as the most illustrative both for the qualitative and quantitative descriptions of characteristic features of cavitating flows. In all plots, the reference point coincides with the leading edge of a foil in the measurement plane at $\alpha = 0°$.

Visualization

Fig. 1 shows typical patterns of partial cavities occurring on the suction side of the plate and NACA0015 foil. In the case of plate, cavitation inception occurs at $\sigma \approx 2.78$ as a bubble-band – an array of bubble-filled streamwise streaks – which differ from the common sheet attached cavity[1] found sometimes behind the leading edge of the foil. Similar streaks were registered by Brandner et al. (2010). The cavity length is $L_C/C = 0.07$. The typical distance between the streaks is about 1 mm. This cavitation pattern persists until approximately $\sigma = 2.26$ (Fig. 1). As the cavitation number is decreased, the streaks become thicker and tend to interact and merge, forming what now may be qualified as an attached streaky-sheet cavity. Here it should be noted that the cavity interface is frothy and, in contrast to results of other papers in the literature (e.g. Franc and Michel, 1985), in the present work the sheet cavity is accompanied by shedding of small (up to $0.02C$) clusters of bubbles at the cavity closure region. This is suspected to be due to either a relatively high level of roughness of the hydrofoil surface or a relatively large (compared to deaerated water) amount of dissolved air in the water.

As well known, a decrease of the cavitation number leads to the growth of the streamwise extent of the cavity and even to transition to another cavity pattern when a certain threshold is overcome. When the cavitation number is decreased to $\sigma = 1.7$ (Fig. 1), the cavity changes to be of transitional type[2]. At this regime, the spatial structure of the cavity is essentially 3D. The cavity length increases up to $L_C/C = 0.23$. Downstream, an increase in local pressure leads to the collapse of micro-bubbles and, consequently, a drop of dispersed-phase concentration. A further decrease of cavitation number results in cloud cavitation[3] (Fig. 1). It is proved that separation of cloud

cavity is accompanied by liquid circulation, which leads to formation of a large-scale vortex around the cloud cavity (Kubota et al., 1989). The characteristic Strouhal numbers for the cloud cavitation regimes are given in the caption of Fig. 1. When $\sigma = 1.14$, the cavity extent grows up to $L_C/C = 1.1$ and the size of detached clouds rises as well.
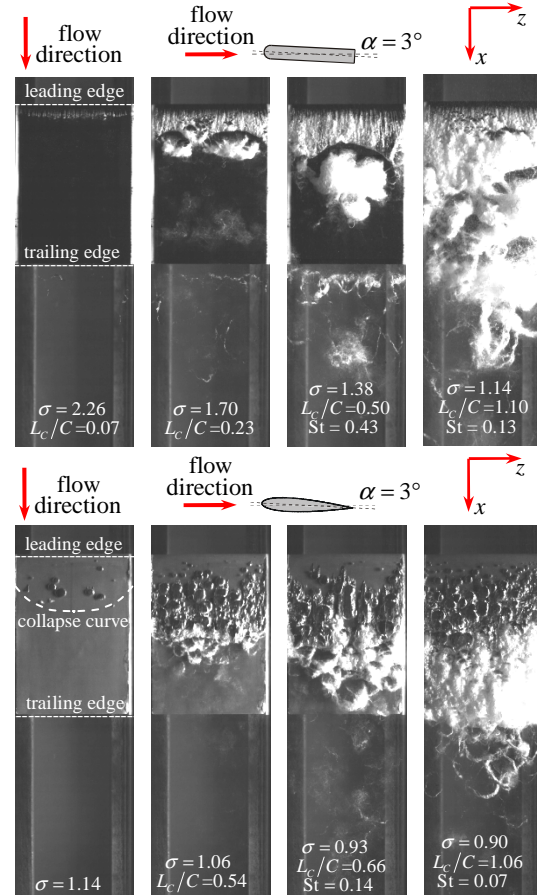
Figure 1. Instantaneous images of partial cavities (top view) on the suction side of the plate (the upper row) and the NACA0015 hydrofoil (the lower row) at $\alpha = 3°$.

In addition, downstream of the plate, one can observe thin streamwise and spanwise structures filled up with vapor and gas. Their origin seems to be connected with generation of strong vortices past the trailing edge of the plate. Inside the cores of those vortices, local pressure most probably falls below the vapor pressure, leading to water vaporization.

In the case of NACA0015 hydrofoil, flow pattern differs significantly. Initially, when $\sigma = 1.14$ separate micro-bubbles arise at a distance of about $0.03C$ downstream from the leading edge of the hydrofoil (Fig. 1). These bubbles are convected downstream with the local fluid velocity of 17.1 m/s. The bubble size grows at a rate of about 5.8 m/s. Such dynamics of bubble growth and movement can be observed until the bubbles collapse further downstream. As suspected, at this threshold location the magnitude of the local pressure reaches the value that

---

[1] Sheet cavity represents a gas-vapor film of a relatively stable length with clear interface. In the region of the sheet cavity closure, the main flow reattaches to the solid surface of the cavitating object.

[2] This cavity type is intermediate between sheet and cloud cavities. In general, at the closure region transitional cavity is accompanied by continuous shedding of relatively small clouds and larger horseshoe-shaped ones consisting of a bulk of gas-vapor micro-bubbles at different parts of the cavity closure region.

[3] As widely acknowledged, cloud cavities are characterized by detachment of the whole cavity from foil surface and quasi-

periodic cloud shedding process due to the appearance of re-entrant jet. A detailed description of cloud cavitation can be found e.g. in Callenaere et al. (2001).

is sufficient to cause the bubble collapse. This cavitation pattern is referred to as the traveling bubble cavitation. At this regime, the cavity is not formed yet.

When the cavitation number becomes lower (Fig. 1), a transitional cavity type can be observed. As in the previous case, the micro-bubbles initiate from the leading edge of the cavity and extend roughly to the hydrofoil half-length. The bubble size varies from zero up to $0.13C$. It should be noted that the cavity leading edge is quite difficult to determine. The trailing part of the cavity is frothy. At the cavity closure region, the bubbles collapse and separate into horseshoe-shaped clouds immediately downstream. These clouds are likely to be situated in the vortex cores and replicate their forms. When σ is about 0.9 (Fig. 1), cloud cavitation occurs. However, as in the case with transitional cavity, one can observe horseshoe-shaped clouds together with the large-scale ones.

Turbulent characteristics

Based on the ensemble of 5000 instantaneous velocity fields in the vertical midplane, the distributions of the mean velocity, turbulent kinetic energy, second- and third-order statistical moments of turbulent fluctuations were calculated over the suction side of the two foils considered. Fig. 2 shows some profiles of the streamwise component of the mean velocity excess over the bulk flow velocity, $(U - U_0)/U_0$, with superimposed isocontours for both foils at the attack angle $\alpha = 3°$ for three different types of cavitation. In the front of the leading edge (not shown here), the flow locally decelerates approaching the stagnation point and the region of slowdown shifts to the pressure side of the foils in all the cases. The mean velocity profiles at $x/C = 0$ are almost identical for all the regimes. Due to the flow deflection and acceleration around the leading edge, the mean velocity reaches soon its maximum above the upper surface of the foils. When σ decreases, the velocity maximum firstly increases and moves downstream but then gradually decreases and shifts upstream. In the case of plate, the reverse shift of the maximum along x-axis, noticed on the hydrofoil, does not occur.

The above findings can be explained in the following way. Unsteady cavity is characterized by pulsations of its closure. Consequently, pulsations at the cavity trailing edge lead to an increase in liquid velocity fluctuations (Fig. 3), more intensive mixing and lateral momentum transfer, which, in turn, reduce the velocity peaks.

Downstream from the region of higher mean velocity along the suction side of the hydrofoils, the mean velocity peaks decrease and eventually disappear, except for the plate at the higher cavitation number (Fig. 2) where at the plate end, $x/C = 1.0$, mild velocity peaks appear again due to the vanishing wall shear at the edge separation. No separation on any of the foils has been detected apart from the trailing edge of the plate. In the case of plate, the transverse dimension of the wake is significantly larger owing to its bluff shape and reaches $0.23C$. This is caused by generation of large-scale vortex structures in the shear layers over the cloud cavity. Here it should be noted that these observations are only for the averaged properties, as the separation points (lines) are not fixed but pulsate around a mean value.

No doubt, hydrodynamic flow separation and the cavitation cloud detachment are interlinked and mutually dependent, but at this stage, it is difficult to portray a clear scenario of this nonlinear interaction. For incipient and mild cavitation, flow separation can be considered as being fully controlled by the hydrodynamics of the carrier fluid, i.e. the adverse pressure gradient on the trailing part of the foil. However, cavitation is always followed by expansion of the gas-vapor phase and the consequent flow acceleration, which will tend to delay flow separation. On the other hand, detachment of cavity clouds have been observed in non-separating flows, though in most cases it is accompanied with re-entrant jet flow underneath, which is indicative of flow separation. It seems plausible, however, that cloud detachment will trigger and promote flow separation and affect its behavior.
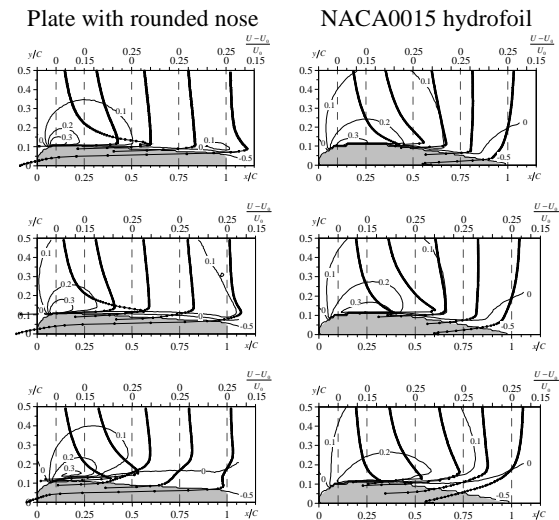
Figure 2. Downstream evolution of the streamwise component of the mean velocity for the plate at (top to bottom) $\sigma = 2.98$ (cavitation-free flow), $\sigma = 2.26$, $L_C/C = 0.07$ (streak cavitation), $\sigma = 1.56$, $L_C/C = 0.3$, St = 0.44 (cloud cavitation) and for the NACA0015 hydrofoil at $\sigma = 1.57$ (cavitation-free flow), $\sigma = 1.14$ (travelling bubbles), $\sigma = 0.93$, $L_C/C = 0.66$, St = 0.14 (cloud cavitation). $\alpha = 3°$.

In general, one can conclude that the velocity fields for the three different cavitation regimes show visible differences illustrating the strong effect of the cavitation of the carrier fluid. Especially the cloud cavitation on both foils (Fig. 2) show conspicuous suppression of velocity peaks over the front part of the foil surfaces due to intensive mixing in the cloud and promotion of early flow separation associated with cloud detachment.

The turbulence statistics shows, as expected, also very strong influence of the cavitation regime and the shape of the test foil. Although all second and third moments are available, the analysis of the turbulence field is confined at present to the streamwise turbulence intensity field. Fig. 3 shows the profiles and isocontours of the r.m.s. of the streamline fluctuations around the two bodies for the same cavitation numbers as in Fig. 2.

As seen in Fig. 3, the r.m.s. of the fluctuations of the streamwise velocity are generally much higher behind the plate in comparison with those on the NACA0015 hydrofoil. For the two higher cavitation numbers corresponding to the noncavitating flow and streaky-sheet or travelling bubbles cavitation in both cases, the turbulence is confined within the attached boundary layer, the outer stream being unaffected. However, for the lower cavitation num-

bers corresponding to cloud cavitation in both cases, the flow separation and cavitation clouds detachment generate intensive velocity fluctuations that spread much beyond the immediate regions around the foils. As shown by Kubota et al. (1989), there is a region of high vorticity inside a cloud cavity, and the small-scale incoherent velocity fluctuations are not uniformly distributed over a cloud cavity but are concentrated near its boundary. Overall, a decrease in the cavitation number leads to a rise in liquid velocity fluctuations. In the flow around the plate, this effect is initially mild (there is almost no visible difference between the r.m.s. profiles and contours for the cavitation-free and streak cavitation cases, Fig. 3). For low cavitation numbers, some wiggles in the turbulence intensity contours downstream (between $x/C = 0.5$ and 0.8), show some secondary higher intensity turbulence spots possibly associated with instabilities induced by the positive pressure gradient.

Plate with rounded nose   NACA0015 hydrofoil
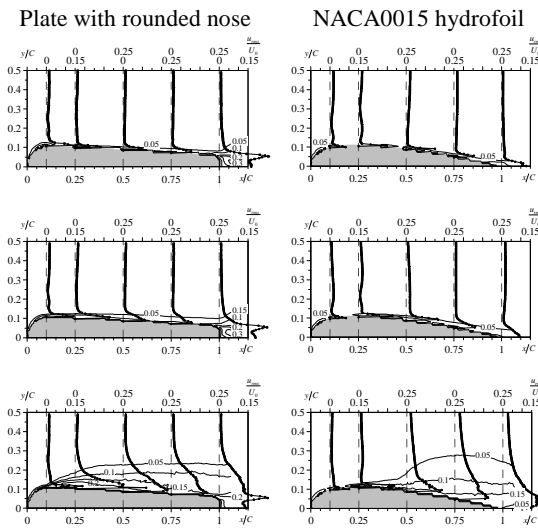
Figure 3. Downstream evolution of streamline turbulence intensity (root-mean-square) for the plate at (top to bottom) $\sigma = 2.98$ (cavitation-free flow), $\sigma = 2.26$, $L_C/C = 0.07$ (streak cavitation), $\sigma = 1.56$, $L_C/C = 0.3$, St $= 0.44$ (cloud cavitation) and for the NACA0015 hydrofoil at $\sigma = 1.57$ (cavitation-free flow), $\sigma = 1.14$ (travelling bubbles), $\sigma = 0.93$, $L_C/C = 0.66$, St $= 0.14$ (cloud cavitation). $\alpha = 3°$.

    Qualitatively a similar pattern is observed also for the NACA hydrofoil, though generally the peaks of turbulence intensity appearing in the thin boundary layer on the foil surface are milder than those in the case of plate. The highest turbulence intensity peaks for all cavitation numbers appear near the trailing edge, which in the case of cloud cavitation (Fig. 3) far exceed the peaks in other two regimes. Again, the difference between the noncavitating flow and travelling bubble cavitation is minor, the latter showing somewhat higher turbulence level especially along the trailing part, presumably enhanced by cavitation. In contrast, just as in the case of plate, the cloud cavitation generates much higher turbulence which spread fast laterally almost up to $y/C = 0.3$.
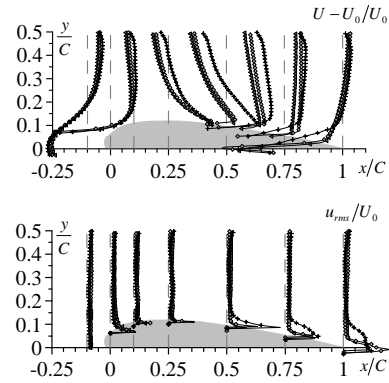
Figure 4. Profiles of (top) the streamwise component of the mean velocity excess over the bulk flow velocity and (below) streamwise turbulence intensity (root-mean-square) for the NACA0015 hydrofoils with different chord length: ◄ – 50 mm, ◊ – 100 mm and + – 200 mm. $\sigma = 1.15$, $\alpha = 3°$.
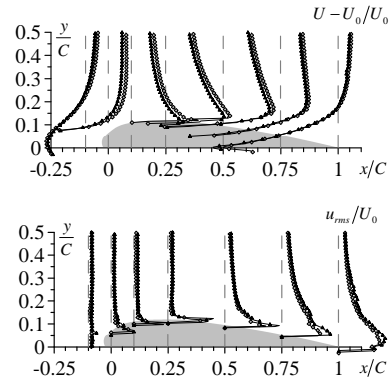
Figure 5. Profiles of (top) the streamwise component of the mean velocity excess over the bulk flow velocity and (below) streamwise turbulence intensity (root-mean-square) for the NACA0015 hydrofoils with different wall roughness: ◊ – 2.8 μm and Δ – 4.5 μm. $\sigma = 0.84$, $\alpha = 3°$.

    Thus, comparing the fields in Fig. 3, one can conclude that transition to the developed cavitation regimes leads to a significant modification of the turbulence level and its distribution. For the plate, the maximum of $\tilde{u}/U_0$ for the cavitation-free case appears at $x/C = 0.28$ and $y/C = 0.1$. Initially, it moves upstream but when transition to cloud cavitation occurs it shifts downstream and increases from 0.13 up to 0.37. However, for the NACA0015 hydrofoil, the maximum of $\tilde{u}/U_0$ shows the same dynamics with a decrease in the cavitation number but occurs slightly downstream compared to the plate. Besides, the increase of the maximum is substantially less compared to the plate: from 0.17 up to 0.22.

    Fig. 4 shows the influence of the foil scale on the mean velocity and turbulence intensity. For the given cavitation number, the regimes presented are transitional for the 200 mm foil, traveling bubbles for the 100 mm foil and noncavitating for the 50 foil. As seen in Fig. 4, velocity distributions coincide before the foils of different scales. However, when the foil leading edge is reached, in the case of the 200 mm foil, longitudinal component of the mean velocity becomes higher compared to the other cases. This is likely caused by flow blockage. Maximum difference of about $0.1U_0$ is achieved between the sections

$x/C = 0.25$ and 0.5. Downstream, the profiles of the mean velocity consist again. Behind the trailing half of the foil, velocity for the 100 mm foil also slightly increases compared to the 50 mm case. Turbulence intensity profiles are noticeably wider (about two times) over the 200 mm foil.

The effect of the wall roughness on the mean and turbulent characteristics of the flow can be estimated from Fig. 5. At $\sigma = 0.84$, cavitation pattern on the foil with 2.8 µm roughness is of transitional type whereas that for the other one is attached streaky-sheet cavity. Thus, one can conclude that, for streak cavitation, the mean velocity over the foil is somewhat less compared to the case of traveling bubbles, though the turbulence intensity is higher due to faster turbulization of the boundary layer. However, for higher cavitation numbers, this effect is significantly less pronounced.

CONCLUSIONS

Visual analysis of high-speed images and PIV measurements of the velocity field and its fluctuations in flows around a flat plate with semi-cylindrical nose and a NACA0015 hydrofoil, both at 3° incidence angle, have been performed for a series of cavitation numbers, corresponding to different cavitation regimes.

Despite a relative similarity of the size and shape of the two foils considered, the cavitation patterns are different. On the plate, the cavitation begins with a bubble band (bubble streak array), arguably governed by flow instability, transition to turbulence and formation of near-wall streamwise vortical streaks with low-pressure core. With a decrease in the cavitation number, streaks merge and transform into a cloud which detaches downstream. In contrast, the process around the NACA hydrofoil begins with travelling bubbles, which, when the cavitation number is decreased, coalesce creating clusters of larger bubbles. The bubble formation takes subsequently a remarkably regular lattice pattern before collapsing into a cloud.

The velocity and turbulence fields for the three different cavitation regimes show visible differences illustrating the strong effect of the cavitation on the carrier fluid. Especially the cloud cavitation on both foils show a notable suppression of the velocity peaks over the front part of the foil surfaces due to intensive mixing in and by the cloud and the promotion of early flow separation associated with cloud detachment. The hydrodynamic flow separation due to adverse pressure gradient and the cavitation-cloud detachment with re-entrant jet underneath are closely related: the separation enhances the cavitation and creation of the cloud, which in turn feeds back into the carrier fluid flow. The progressive growth of gas-vapor cavity promotes early separation by shifting the separation point upstream, as well as more intensive recirculation. The cloud cavity leads to formation of an intense turbulent wake behind the cavity closure region, significantly extended in the transverse extent, as well as significant intensification of turbulent fluctuations due to strong shear at the cloud edges and generation of large-scale vortical structures over the vapor cavity. Thus, the transition to cloud cavitation leads to global modification of the flow and turbulence and significant changes in the flow pattern as compared to the cavitation-inception case.

Additionally it was shown that the larger hydrofoil is, the wider the turbulent wake is past the foil. This is caused by the flow acceleration above the foil surface due to greater flow blockage in comparison with the cases of smaller foils. An increase of the hydrofoil surface roughness leads, however, to faster boundary layer turbulization and, therefore, to change of cavitation pattern on the foil suction side.

REFERENCES

Akhmetbekov, Ye. K., Bilsky, A. V., Lozhkin, Yu. A., Markovich, D. M., Tokarev, M. P., and Tyuryushkin, A. N., 2006, "Software for experiment management and processing of data obtained by digital flow visualization techniques (ActualFlow)", *Numerical Methods and Programming*, Vol. 7, pp. 79-85 (in Russian).

Brandner, P. A., Walker, G. J., Niekamp, P. N., and Anderson, B., 2010, "An experimental investigation of cloud cavitation about a sphere", *Journal of Fluid Mechanics*, Vol. 656, pp. 147-176.

Callenaere, M., Franc, J.-P., Michel, J.-M., and Riondet, M., 2001, "The cavitation instability induced by the development of a re-entrant jet", *Journal of Fluid Mechanics*, Vol. 444, pp. 223-256.

Cervone, A., Bramanti, C., Rapposelli, E., and d'Agostino, L., 2006, "Thermal cavitation experiments on a NACA 0015 hydrofoil", *ASME Journal of Fluids Engineering*, Vol. 128, pp. 326-331.

Coutier-Delgosha, O., Devillers, J.-F., and Pichon, T., 2006, "Internal structure and dynamics of sheet cavitation", *AIP Physics of Fluids*, Vol. 18, (017103)-12.

Franc, J.-P., and Michel, J.-M., 1985, "Attached cavitation and the boundary layer: experimental investigation and numerical treatment", *Journal of Fluid Mechanics*, Vol. 154, pp. 63-90.

George, D. L., Iyer, C. O., and Ceccio, S. L., 2000, "Measurement of the bubbly flow beneath partial attached cavities using electrical impedance probes", *ASME Journal of Fluids Engineering*, Vol. 122, pp. 151-155.

Laberteaux, K. R., and Ceccio, S. L., 2001, "Partial cavity flows. Part 1. Cavities forming on models without spanwise variation", *Journal of Fluid Mechanics*, Vol. 431, pp. 1-41.

Kawanami, Y., Kato, H., Yamaguchi, H., Tagaya, Y., and Tanimura, M., 1997, "Mechanism and control of cloud cavitation", *ASME Journal of Fluids Engineering*, Vol. 119, pp. 788-795.

Kravtsova, A. Yu., Markovich, D. M., Pervunin, K. S., and Timoshevskiy, M.V., 2012, "Turbulent structure of cavitating flows about 2D model bodies", *Proceedings, 8th International Symposium on Cavitation*, pp. 450-455.

Kubota, A., Kato, H., Yamaguchi, H., and Maeda, M., 1989, "Unsteady structure measurement of cloud cavitation on a foil section using conditional sampling technique", *ASME Journal of Fluids Engineering*, Vol. 111, pp. 204-210.